energy&fuels

Article

pubs.acs.org/EF

Autoignition Characterization of Primary Reference Fuels and *n*-Heptane/*n*-Butanol Mixtures in a Constant Volume Combustion Device and Homogeneous Charge Compression Ignition Engine

Marc E. Baumgardner,[†] S. Mani Sarathy,[‡] and Anthony J. Marchese*,[†]

[†]Colorado State University, Fort Collins, Colorado 80523, United States of America

[‡]Clean Combustion Research Center, King Abdullah University of Science and Technology, Thuwal, Kingdom of Saudi Arabia

ABSTRACT: In this study, the autoignition behavior of primary reference fuels (PRF) and blends of *n*-heptane/*n*-butanol were examined in a Waukesha Fuel Ignition Tester (FIT) and a Homogeneous Charge Compression Engine (HCCI). Fourteen different blends of iso-octane, *n*-heptane, and *n*-butanol were tested in the FIT—28 test runs with 25 ignition measurements for each test run, totaling 350 individual tests in all. These experimental results supported previous findings that fuel blends with high alcohol content can exhibit very different ignition delay periods than similarly blended reference fuels. The experiments further showed that *n*-butanol blends behaved unlike PRF blends when comparing the autoignition behavior as a function of the percentage of low reactivity component. The HCCI and FIT experimental results favorably compared against single and multizone models with detailed chemical kinetic mechanisms—both an existing mechanism as well as one developed during this study were used. The experimental and modeling results suggest that that the FIT instrument is a valuable tool for analysis of high pressure, low temperature chemistry, and autoignition for future fuels in advanced combustion engines. Additionally, in both the FIT and engine experiments the fraction of low temperature heat release (fLTHR) was found to correlate very well with the crank angle of maximum heat release and shows promise as a useful metric for fuel reactivity in advanced combustion applications.

1. INTRODUCTION

The urgent need to increase efficiency and reduce exhaust emissions from internal combustion engines has resulted in an increased interest in High Efficiency Clean Combustion (HECC) engines. Premixed or partially premixed compression ignition modes, such as homogeneous charge compression ignition (HCCI),[1] reactivity controlled compression ignition (RCCI),[2] and multizone stratified compression ignition (MSCI)[3] have been a particular focus because of their potential to deliver enhanced fuel efficiency and meet exhaust emissions mandates without the addition of costly after-treatment technologies.[4] Many advanced internal combustion engine concepts such as HCCI, RCCI, MSCI, and other similar strategies, rely on a premixed or partially premixed autoignition event, which is typically governed by low temperature chemical kinetics. Many researchers have shown that combustion strategies such as HCCI or MSCI are more amenable to moderately reactive fuels (i.e., low to moderate octane number).[1,3,5,6] However, research has also shown that existing autoignition metrics such as octane number (ON) or cetane number (CN) are not directly applicable toward characterizing autoignition under homogeneous premixed or partially premixed conditions.[5,7−10] Accordingly, new fuel characterization methods and autoignition metrics must be developed that are applicable to future fuels in advanced combustion modes. Recently, there have been several approaches to characterizing fuel performance and rank in HCCI (and other HECC engine modes). These approaches have produced various levels of success but ultimately do not adequately address the characteristics of future fuels. So, there exists a need to further develop a more precise understanding of the role of low temperature reactivity in the combustion phasing of potential future fuels within HECC engines and to determine if any correlation can be made that helps to better rank and order these fuels.

In recent years, the Ignition Quality Tester (IQT) has seen increased use as a fundamental combustion research tool because of its ability to rapidly measure the ignition delay of a variety of fuels at low to intermediate temperature.[8,11−13] Bogin et al.[14] have recently shown that ignition delay periods for various heptane isomers tested in an IQT show similar behavioral trends as the same fuels tested in a homogeneous rapid compression machine (RCM) by Silke et al.[15] Bogin et al. modeled the IQT with KIVA-3 V and several reduced chemical kinetic mechanisms and concluded that the ignition behavior was dominated by chemical kinetic effects as compared to spray physics. Bogin et al. also suggested that the dominance of chemical kinetics increased substantially for fuels with longer ignition delay periods.[12] Perez et al. further showed that fuels possibly best suited for HCCI such as those with a RON of approximately 70 exhibit IQT ignition delay periods of greater than ∼8 ms, which is sufficiently long for the system to be modeled homogeneously.[8] Perez and co-workers tested a wide range of gasoline-like fuels to determine if HCCI autoignition behavior could be predicted or correlated to that measured in an IQT. They tested 21 different surrogate gasoline fuels in an IQT and an HCCI engine and found that the inverse of ignition delay period correlated relatively well with the CA50 data (i.e., the point of 50% total heat release, which is indicative of

Received: August 9, 2013
Revised: November 5, 2013
Published: November 18, 2013

primary ignition) from the HCCI engine. Perez and co-workers also found that, while the inverse of ignition delay periods generally correlated with the RON and Octane Index (OI), there were substantial differences between fuels of the same RON that could not be explained by either the RON or OI scales.

This study focuses on determining if differences in HCCI performance can be predicted or explained by interpreting results from an FIT. The autoignition behavior of primary reference fuels (PRF) and blends of *n*-heptane/*n*-butanol were examined in a Waukesha Fuel Ignition Tester (FIT) and compared against experiments in a Homogeneous Charge Compression Engine (HCCI). Fourteen different blends of iso-octane, *n*-heptane, and *n*-butanol were tested in the FIT. The experimental results presented herein support previous findings that fuel blends with high percentages of alcohols can exhibit very different ignition delay periods in comparison to traditional petroleum fuels. The results further suggest that *n*-butanol blends behave unlike PRF blends when comparing the autoignition behavior as a function of the percentage of low reactivity component (e.g., butanol vs iso-octane) and that these differences persist whether volume or molar percentages are considered. The HCCI and FIT experimental results were compared against single and multizone models using detailed chemical kinetic mechanisms for PRF and *n*-butanol mixtures. To support these computations, a new *n*-butanol/*n*-heptane chemical kinetic model is presented that exhibits good agreement with the experimental FIT and HCCI data. The results also suggest that that the FIT instrument is a valuable tool for analysis of high pressure, low temperature chemistry, and autoignition for future fuels in advanced combustion engines. In fact, in both the FIT and engine experiments, the fraction of low temperature heat release (fLTHR) was found to correlate very well with the crank angle of maximum heat release and shows promise as a useful metric for fuel reactivity in advanced combustion applications.

2. METHODS

2.1. Fuel Ignition Tester. In this study, a Waukesha FIT was used to examine the reactivity of blends of *n*-butanol and *n*-heptane. These blends were then compared to equal volumetric blends of PRF. The FIT (schematic diagram in Figure 1) is a constant volume combustion chamber device that allows a systematic determination of a derived cetane number (DCN) according to ASTM D7170[16] and is very similar to the Ignition Quality Tester,[8,12,14] which also measures DCN according to its own ASTM standard (D6890).[17] The ASTM D7170 method uses the following correlation based on the measured ignition delay (ID) period after injection of a liquid fuel into the combustion chamber:

$$\text{FIT DCN} = \frac{171}{\text{ID[ms]}} \quad (1)$$

The FIT operating temperature and pressure range, shown in Table 1, are ideal for examining the prominent low temperature combustion region of an HCCI engine as shown in the red box in Figure 2a. Figure 2b is an example FIT pressure trace showing the average of 25 injections compromising one test for pure *n*-butanol. Note that the FIT measures "ignition" once the in-vessel pressure rises +0.2 bar above the injected pressure. The operation of the FIT is further explained in section 3.

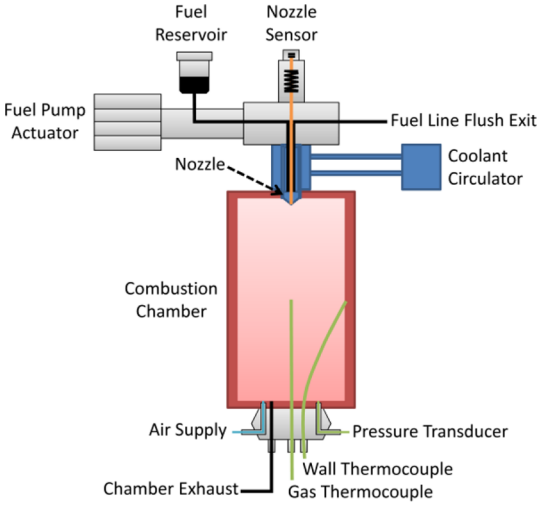

Figure 1. Schematic diagram of Fuel Ignition Tester adapted from ASTM D7170.[16]

Table 1. Nominal Operating Parameters for the Waukesha FIT Apparatus (per ASTM D7170)

volume	0.6 L
pressure	24 bar
wall temp.	580 °C (853 K)[a]
global equivalence ratio	0.1–0.6

[a]Note that chamber gas temperature was measured as 32 ± 10 °C lower than the user-defined wall temperature.

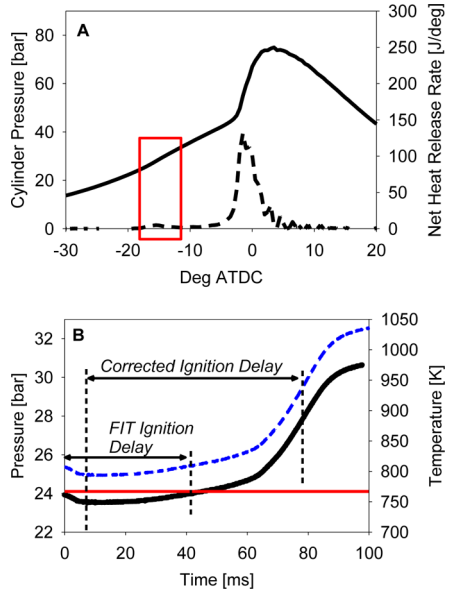

Figure 2. FIT and HCCI similarities: (a) a HCCI engine data showing pressure and net heat release rate (from the present study). The red box shows that the region of low temperature chemistry seen in the experimental HCCI engine is in the same range as that tested in an FIT. The solid line is the pressure trace for nBuOH40 and the dotted line is the net heat release rate. The test conditions were 60%v *n*-butanol/40%v *n*-heptane at φ of 0.33, T_{in} of 70 °C, P_{in} of 1.0 bar, 1500 rpm and 16:1 compression ratio. (b) Pressure trace average (black line) for a typical *n*-butanol ignition test in the FIT, calculated temperature (dashed blue line), and the FIT trigger point (red line).

2.2. HCCI Engine. To demonstrate the performance of the proposed fuel blends in HCCI mode, a diesel engine was converted for use as an HCCI test bed. Specifically, one cylinder of a John Deere PowerTech 2.4L 4024 turbo-diesel engine was modified to operate in HCCI mode. The existing in-cylinder fuel injector was disconnected in

dx.doi.org/10.1021/ef4015982 | Energy Fuels 2013, 27, 7778–7789

favor of using port fuel injection (via a gasoline-type injector located approximately 50 cm upstream of the intake valve) to produce a homogeneous mixture of air and fuel that is typical of HCCI operation. The in-cylinder pressure was measured using a Kistler 6056A pressure transducer and data were recorded every 0.5 °CA, which was the resolution for the crank angle sensor used in this study.

The net heat release rate was calculated via a standard, first law analysis often used in literature[18] and based on eq 2:

$$\frac{dQ}{dt} = \frac{\gamma}{\gamma - 1} p \frac{dv}{dt} + \frac{1}{\gamma - 1} v \frac{dp}{dt} \quad (2)$$

where γ is the ratio of specific heats, p the pressure, and v the instantaneous cylinder volume. The heat release rate was computed assuming that the combustion gas was primarily air modeled as an ideal gas but including the temperature dependence of γ. It should also be noted that the heat release rates shown herein are not filtered but rather slightly smoothed as a result of numerical integration and the fact that the results shown represent an average of 100 consecutive cycles.

Additional modifications to the engine consisted of alterations to the intake and exhaust manifolds to allow isolation of the HCCI cylinder and the installation of an air preheater necessary to achieve the higher intake temperatures typically associated with HCCI operation.[1,19] The intake heater was controlled within ±2 °C of the desired temperature (70 °C) for all tests via a custom National Instruments interface. The piston head of the HCCI cylinder was also modified such that the compression ratio could be adjusted to allow HCCI tests at various compression ratios. Specifically, the bowl of the piston was milled down flat resulting in a compression ratio of 12:1. Various size disks were then bolted into the milled out pocket to increase the compression ratio up to a maximum of 18:1. For the results presented herein, the 16:1 compression ratio piston configuration was used. The specifications of the HCCI engine are detailed in Table 2.

Table 2. Homogeneous Charge Compression Ignition Engine Parameters for the Experiments Presented Herein

displacement vol.	609 cm^3
compression ratio	16:1
speed	1500 rpm
intake temp.	70 °C (343 K)
intake pressure	1.0 bar
bore	86 mm
stroke	105 mm
global fuel−air equivalence ratio	0.33

2.3. Fuels and Chemical Kinetic Models. Future fuels with desired properties for optimal performance in advanced combustion modes will most likely consist of mixtures of petroleum derived products (aromatics, straight and branched alkanes), alcohols, synthetic alkanes (straight and branched alkanes produced from natural gas, vegetable oil, or animal fat), fatty acid methyl esters, and natural gas (liquefied or compressed). Fuel blends such as these (with properties currently tailored for compression-ignition or spark-ignition engines) are beginning to see increased penetration into the global transportation fuel market. For example, the U.S. currently mandates a 10%v minimum ethanol blending requirement for gasoline and the U.S. Environmental Protection Agency (EPA) recently reported that mixtures up to 15%v will be considered for future blends.[20]

Butanol has received much attention in recent years as a bio-alternative to ethanol because of its higher energy density and higher miscibility with other hydrocarbons. There have also been a wide array of chemical kinetic studies of butanol (and its isomers) recently, and well-validated experimental data and chemical mechanisms exist.[21,22,24,28,29]

Table 3 shows the physical properties of the fuel mixtures used in this study. Viscosity, density, and bulk modulus measurements were performed by the authors. The viscosity and density were measured via an Anton Paar SVM 3000 Stabinger Viscometer instrument. The bulk modulus (BM) was calculated via density and speed of sound measurements carried out with an Anton Paar DSA 5000M. Bulk modulus was determined as it is a well-known physical property that can affect fuel injection and timing in cases, such as ours, where there is some significant distance between the fuel pump and the injector (such as for pump line diesel injectors or some rare configurations of unit injectors).[30−33]

Accompanying the experimental data, zero-dimensional (single and multizone) models were performed using the CHEMKIN[36] and CHEMKIN-PRO[37] chemical kinetic modeling packages. For comparison, several chemical kinetic mechanisms were used to examine the experimental results. For the *n*-butanol fuel blends, mechanisms developed by Saisirirat et al.[23] and Sarathy et al. were used. The Saisirirat et al.[27] mechanism was chosen since it was one of the very few available mechanisms, which included a well-tested *n*-heptane submechanism. Several important distinctions exist between these two mechanisms, which are detailed in Table 4. Primarily, it is important to note that while engine experiments were performed by Saisirirat et al.,[23] no engine modeling was done to directly correlate against their data. Rather, the engine experiments were used to qualitatively interpret the mechanism. Therefore, the ignition behavior predicted by the Saisirirat et al. mechanism is based primarily on chemistry derived from Jet Stirred Reactor (JSR) data. Conversely, the Sarathy et al.[23] mechanism has been validated against a very large data set, including some of the JSR data from Saisirirat et al. as well as ignition experiments in both shock tubes and rapid compression machines.

However, as mentioned above, the Saisirirat et al. mechanism does include an *n*-heptane submechanism, while the Sarathy et al. mechanism does not. Accordingly, for the present study, the authors have combined the *n*-heptane submechanism from Mehl et al.[38] with

Table 3. Properties of Fuels Considered in This Study

fuel	*n*-butanol [vol %]	*n*-heptane [vol %]	*i*-octane [vol %]	viscosity [mm^2/s]	density [g/cm^3]	bulk modulus [kN/m^2][a]	RON	DCN
nC7	0	100		0.442	0.684	909	0	54.1
nBuOH20	20	80		0.584	0.708	950		40.5
nBuOH40	40	60		0.805	0.734	1019		24.6
nBuOH60	60	40		1.144	0.760	1095		16.5
nBuOH80	80	20		1.623	0.785	1185		10.5
nBuOH95	95	5		2.090	0.804	1257		5.4
nBuOH	100	0		2.248	0.810	1279	96[b]	3.7
PRF20		80	20	0.449	0.686	896	20	47.8
PRF40		60	40	0.462	0.687	884	40	42.4
PRF60		40	60	0.484	0.689	870	60	36.8
PRF80		20	80	0.507	0.690	856	80	28.4
PRF95		5	95	0.529	0.692	846	95	20.5
PRF100		0	100	0.542	0.692	842	100	11.1

[a]Bulk modulus was calculated based on viscosity and speed of sound measurements. [b]*n*-butanol RON value from refs 34 and 35.

dx.doi.org/10.1021/ef4015982 | Energy Fuels 2013, 27, 7778−7789

Table 4. Chemical Kinetic Mechanisms for *n*-Butanol, *n*-Heptane, and iso-Octane Blends Used in This Study and the Data Sets Against Which These Mechanisms Have Been Validated

mechanism	species	reactions	relevant fuel mixtures	experimental apparatus	temp. range	pressure range	equivalence ratios
Saisirirat et al.[a]	1046	4398	20/80 mol nBuOH/nC7 50/50 mol nBuOH/nC7	jet stirred reactor	530−1070 K	10 atm	0.3, 0.5, 1
			100%v *n*-heptane 18%v nBuOH in nC7 37%v nBuOH in nC7 57%v nBuOH in nC7	HCCI Engine: 1 of 4 cyl diesel engine motored at 1500 rpm	80 °C intake temp.	n/a	0.3
Sarathy et al.[b]	426	2335	100% nBuOH	laminar flame measurements	353 K	1 atm	0.6−1.6
			100% nBuOH	Flat Flame	n/a	40 mbar	1.7
			100% nBuOH	flat flame	n/a	15 Torr	1.0
			100% nBuOH	shock tube	770−1250 K	10−80 atm	1.0
			100% nBuOH	shock tube	1050−1600 K	1.5−43 atm	0.5,1.0
			100% nBuOH	rapid compression machine	725−855 K	15 atm	0.5, 1.0, 2.0
			100% nBuOH	jet stirred reactor	530−1070 K	10 atm	0.5, 1.0, 2.0

[a]Data for Saisirirat et al.[23,40,41] [b]Data for Sarathy et al.[21,25−27,42−45]

the Sarathy et al.[27] *n*-butanol mechanism, and further present some comparisons of this model against the experimental data detailed in section 3. To merge the *n*-heptane model of Mehl. et al. mechanism to the existing Sarathy et al. mechanism, duplicate species and reactions were identified and removed, ensuring consistency in the base mechanisms and maintaining the predictive capabilities of the pure butanol and pure heptane models. No cross reactions were considered since interactions between the two fuels primarily occur via the smaller radicals generated from the parent fuels. It should also be noted that the Mehl et al.[39] mechanism represents an update of the Curran et al. PRF model, which is the PRF submechanism used in the Saisirirat et al. mechanism.[23]

3. RESULTS AND DISCUSSION

3.1. FIT Experimental Results. Fourteen different blends of iso-octane, *n*-heptane, and *n*-butanol were tested in the FIT, consisting of 28 test runs with 25 ignition measurements for each test run, totaling 350 individual tests. Figure 3 summarizes these test results, wherein *n*-heptane is the "high reactivity fuel" and *n*-butanol or iso-octane are the "low reactivity" fuels. As noted above, the FIT records a derived cetane number (DCN), which generally varies inversely with RON[46] insofar as fuels with high RON exhibit low DCN and vice versa.

It should be noted here that the FIT (similar to the IQT) reports the ignition delay period based on an internal threshold response to the combustion pressure rising a set amount (+0.2 bar for the FIT) above the base pressure (see Figure 2b). This technique can produce erroneous ignition delay periods since low temperature chemistry can result in a small pressure rise prior to primary ignition. For the high reactivity diesel fuels that these devices were originally designed to accommodate, the low temperature pressure rise is not problematic for DCN measurements since it occurs at time periods very close to that of the primary ignition event. However, for fuels with longer ignition delay periods such as those tested in the present study, the low temperature pressure rise can be misinterpreted as the primary ignition event. Additionally, there is a decrease in system pressure and temperature due to fuel vaporization, which is also evident in Figure 2b. Accordingly, we report here both the FIT-reported ignition delay period and an ignition delay period calculated as the time from minimum pressure to the peak pressure rise rate (PPR). Both ignition delays periods along with the model results are presented in Section 3.2.

The present results further show that the injected fuel-air global equivalence ratio (herein referred to as φ) changes due

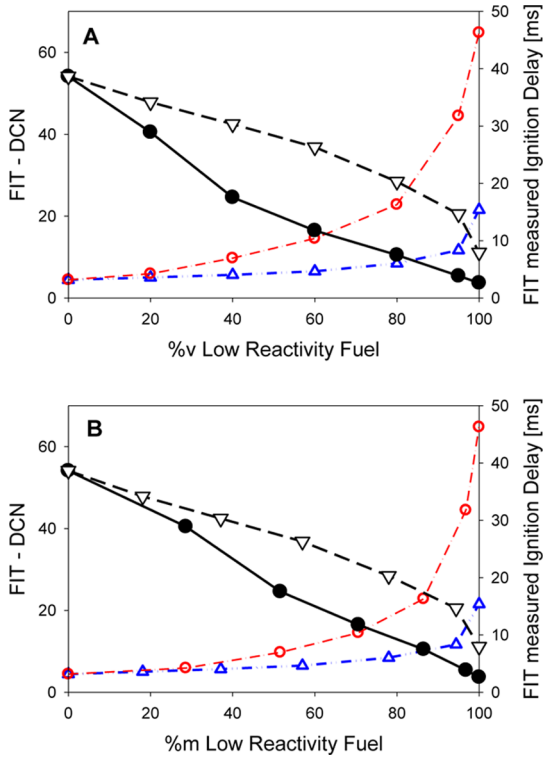

Figure 3. FIT derived cetane numbers for blends of *n*-heptane/*n*-butanol (closed circle, solid line) and *n*-heptane/iso-octane (open triangle down, dashed line) per ASTM D7170 as a function of the percentage of low reactivity fuel component presented on a (a) volume basis and (b) molar basis. Additionally shown are the corresponding FIT measured ignition delay periods used to calculate the DCN values shown: *n*-heptane/*n*-butanol (open circle, dash-dot red line) and *n*-heptane/iso-octane (open triangle up, dash-dot-dot blue line).

to the near constant volume injection style of the FIT and the different physical properties of the fuels tested herein. In Figure 4 the measured fuel density is plotted against the average value of the global equivalence ratio tested for each fuel mixture. To determine a global equivalence ratio for a given test, the fuel was weighed before and after each test and the resulting mass difference was averaged over the 27 injections for that test. The FIT is equipped with a pressurized air system that is used to purge all the lines before and after a test.

dx.doi.org/10.1021/ef4015982 | *Energy Fuels* 2013, 27, 7778−7789

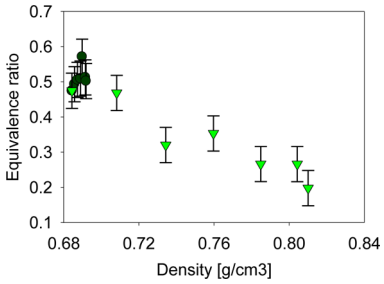

Figure 4. Injected global equivalence ratio as a function of density for PRF (circles) and nBuOH blends (triangles).

The fuel was gravimetrically weighed using a standard high precision scale (accurate to 0.001g) before and after each set of 27 injections. The built-in air purge system allowed the authors to ensure the system was purged completely prior to weighing each sample. Next, the amount of air for each test was calculated based on ideal gas assumptions and the individual injection temperature and pressure readings. Note that the assumption of ideal gas was compared vs both Peng−Robinson and Lee-Kesler real-gas methodologies and deviation from ideal gas assumption was less than 1% error. It is observed that, for the PRF fuels, the tested φ is essentially constant at a value of approximately 0.5, whereas the tested φ changes for the nBuOH mixtures from approximately 0.2 to 0.5. Efforts to understand how the FIT can modulate φ are underway but for this study the experimentally determined φ values were used for the modeling results.

The experimental results in Figure 3 support previous findings that fuel blends with significant amounts of alcohols can exhibit very different ignition delay periods in an IQT or FIT[11] as compared to traditional petroleum fuels. The present experiments further show that *n*-butanol blends behaved unlike PRF blends when comparing the autoignition behavior (e.g., DCN values) as a function of the percentage of low reactivity component. Some of this behavior could be due to the tertiary carbon in iso-octane where the increased number of primary sites in iso-octane, on which the H-atom abstraction rate by OH is lower than secondary sites in *n*-alkanes. Similar results were seen with t-butanol in an IQT study by Haas et al.[11] In the Haas et al. study, the concave down-like behavior of t-butanol/*n*-heptane blends was attributed to a lower OH hydrogen abstraction rate from t-butanol (compared to primary and secondary butanols), thus allowing more OH to be present to attack the base *n*-heptane fuel. This behavior led to generally shorter ignition delay periods for t-butanol blends in comparison to the other three butanol isomers considered by Haas, et al.[11] Alternatively, the *n*-butanol competed relatively equally with *n*-heptane for the OH radicals, resulting in a more linear trend in observed DCN as a function of molar blending percentage. The latter result was also observed in the FIT results presented here in Figure 3.

3.2. FIT Modeling Results. For the *n*-butanol/*n*-heptane blend simulations, the Sarathy et al.[27] mechanism was updated with the *n*-heptane submechanism from Mehl et al.,[38] which is a well-validated mechanism that has been used for modeling gasoline surrogate fuels such as PRF's. The Mehl et al. mechanism was also used to simulate the PRF FIT experiments. Hereafter, the modified Sarathy et al. mechanism (which includes the *n*-heptane submechanism from Mehl et al.) will be referred to as the Sarathy* mechanism. Figure 5 shows plots of

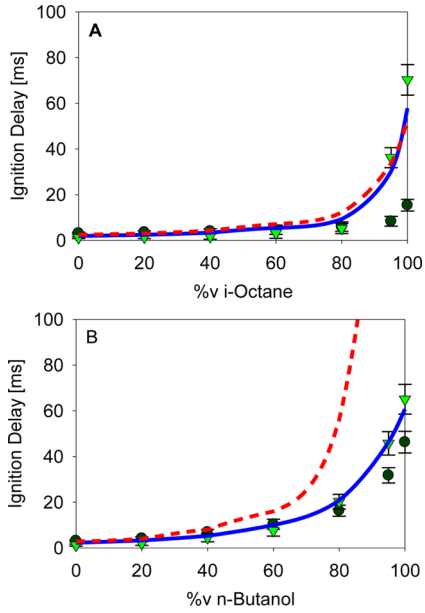

Figure 5. Ignition delays for (a) PRF blends and (b) nBuOH blends. Shown are the ignition delays reported by the FIT (circles), ignition delay found as time from minimum pressure/temperature to max dP/dt (triangles), the Sarathy*/Mehl mechanism prediction (blue solid line), and Saisirirat et al. mechanism prediction (red dashed line).

measured and predicted FIT ignition delay period data for PRF fuels and *n*-butanol/*n*-heptane blends.

For the modeling results presented in Figure 5 a single-zone, constant volume model with heat transfer model was used. One important issue was developing an appropriate heat transfer correlation for the FIT instrument. Due to the similar nature both in injection and pressure/temperature range to a diesel engine, the Taylor correlation[47] for the Nusselt number was used following the arguments set forth in Ferguson and Kirkpatrick:[48]

$$\mathrm{Nu} = 10.4\mathrm{Re}^{0.75} \quad (3)$$

To use this correlation, a characteristic speed had to be determined to calculate the Reynolds number. It was decided to use the speed at which mixing occurs since this is somewhat representative of the turbulence within the vessel. From a review of our own vaporization times (i.e., the time from initial injection to minimum pressure) and reported mixing times for the IQT[12,14] along with the diameter of the FIT combustion chamber, an average speed of 20 m/s was chosen to calculate the Reynolds number in eq 3. Thus, with eq 3 and average properties of air at the initial FIT temperature and pressure a heat transfer coefficient of approximately 600 W/(m^2 K) was used in the CHEMKIN FIT modeling. This value is about half to one-fourth that found in HCCI engine heat transfer studies.[49,50] To evaluate the sensitivity of these calculations to the heat transfer coefficient, adiabatic simulations as well as simulations with double the heat transfer coefficient (i.e., 1200 W/(m K) were also performed. These calculations resulted in only a 3.8% variation in the calculated ignition delay period. Therefore, it was determined that the simulations were relatively insensitive to the value of the heat transfer coefficient. This heat transfer coefficient is admittedly somewhat simplified and reflects some lumping of the heat transfer into a single parameter and accounting for the turbulence introduced by not only fuel injection but also the purging and filling of the vessel with air between injections.

dx.doi.org/10.1021/ef4015982 | *Energy Fuels* 2013, 27, 7778−7789

The initial model conditions were chosen to coincide with an average value of minimum pressure and temperature in the FIT after fuel injection of 800 K and 23.5 bar, respectively. The general CHEMKIN model conditions for the FIT were then kept constant for both the PRF and nBuOH simulations. The only changes made from the PRF to the nBuOH model calculations were the aforementioned φ value changes based on experimentally determined values. Note that the model predictions from both mechanisms compare favorably for PRF blends but diverge when applied to the nBuOH mixtures.

The Sarathy* mechanism agrees well with the experimental data for all injection timings. Note that previously, Bogin et al.[12] showed that the IQT could only be considered effectively homogeneous at ignition delays longer than ~20 ms, the implication being that simulations assuming homogeneous conditions would deviate from experimental results at short ignition delay periods. This result is consistent with those obtained in the FIT. However, simulation errors at low ignition delay periods can vary by a large percentage and still be within a few milliseconds of the actual value. Therefore, the observable error is somewhat lessened by the nature of the experimental and simulation conditions.

3.3. HCCI Engine Experiments and Modeling. HCCI engine experiments were also performed and simulated using the same chemical kinetic mechanisms. For this study, six different fuels that span a wide range of reactivity but still ignite under the HCCI conditions of Table 5 were chosen for comparison. After base-lining the simulations against experimental data, simulations for the entire range of blended fuels in this study were performed and used to support the phenomenological argument proposed in section 3.5.

Table 5. Fuels Tested in the HCCI Engine

fuels	%M LRF[a]	fLTHR[b]	CA50
nC7	0	0.106	−9
PRF 40	37.1	0.067	−3.5
PRF 50	48.9	0.045	0.5
nBuOH40	51.6	0.044	−1
nBuOH50	61.5	0.040	1.5
nBuOH60	70.6	0.018	7.5

[a]Molar percent of low reactivity fuel. [b]fractional low temperature heat release.

Figure 6 is a plot of the measured instantaneous cylinder pressure and apparent rate of heat release for nBuOH40 and PRF40 fuels operating in the HCCI engine under the conditions listed in Table 2. Comparing this data to that in Figure 3, it is apparent that under both engine and FIT conditions the nBuOH40 fuel is found to ignite after the PRF40. This result is consistent with predictions based on the FIT data that suggest nBuOH40 is less reactive than PRF40. Though the trends are similar, the difference in ignition delay is not as great in the HCCI engine as that observed in the FIT. This result can be attributed to the fact that the temperature and pressure in an engine are constantly rising from intake valve closure to near top dead center; and so, ignition differences, which may be large at low temperature, manifest themselves more subtly as the accumulated effects of differences when the temperatures and pressures vary throughout the engine cycle. The effects of heat losses are also greater in the engine, so heat released as a result of chemical reactions do not lead to thermal runaway (i.e., ignition) at the same rate as in the FIT.

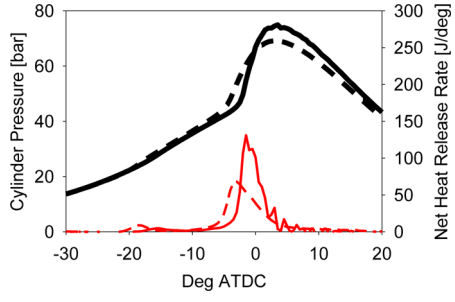

Figure 6. HCCI engine data for nBuOH40 (solid lines) and PRF40 (dashed lines). Shown are cylinder pressure (thick black lines) and net heat release rate (thin red lines) for HCCI test conditions listed in Table 2.

For all the single-zone CHEMKIN models, the in-cylinder temperature was slightly adjusted (+7 °C from measured intake conditions) to account for in-cylinder vs intake conditions as well as to improve the agreement for both models. The initial conditions were then kept constant for all subsequent models to maintain consistency with the experimental tests. Note that this section contains only the single-zone modeling results. Multizone modeling results are presented in section 3.3.1.

Figures 7 and 8 are comparisons between the HCCI engine data and single-zone modeling results. The figures include the instantaneous in-cylinder pressure data, along with the instantaneous net rate of heat release calculated from the in-cylinder pressure data per eq 2. Figures 7b, and 8b focus more closely on the low temperature component of the instantaneous net rate of heat release. Although single-zone models are known to not accurately capture the pressure rise rate within the system,[1,51] these simulations are an effective means of evaluating a mechanism's ability to capture ignition timing as well as the relative differences of ignition timing between different fuels. Moreover, the single-zone computations are also effective in isolating the chemical kinetic differences between different mechanisms under the same operating conditions (e.g., temperature, pressure and engine speed).

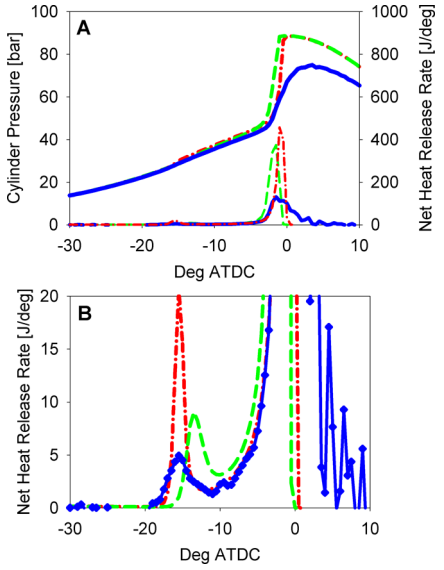

Figure 7. HCCI data for nBuOH40 (solid blue line) vs model data from Sarathy* (green dashed line) and Saisirirat et al. (red dash-dot-dash line); (a) pressure (upper set of curves) and net heat release rate (lower set of curves), and (b) low temperature heat release.

dx.doi.org/10.1021/ef4015982 | Energy Fuels 2013, 27, 7778−7789

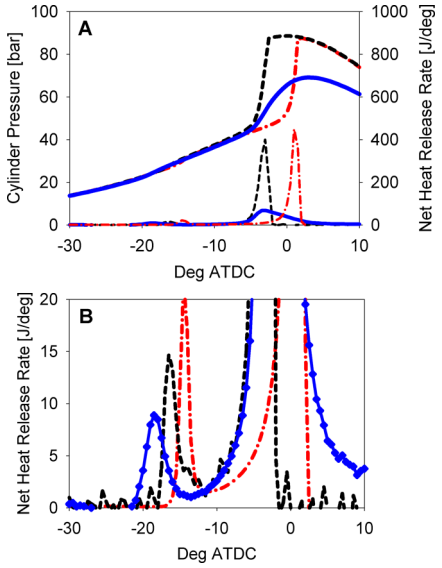

Figure 8. HCCI data for PRF40 (solid blue lines) vs model data from Mehl et al. (dashed black line) and Saisirirat et al. (red dash-dot-dash line); (a) pressure (upper set of curves) and net heat release rate (lower set of curves), and (b) low temperature heat release.

In all cases, the single-zone models overpredicted the magnitude of the heat release and the peak pressure, which is expected with a zero-dimensional, single-zone model since it does not take into consideration the inhomogeneity of actual equivalence ratio or temperature gradients within the cylinder. Use of multizone modeling has proven to be very accurate at matching pressure and heat release profiles[51,52] and is explored further in the next section.

3.3.1. Multi-Zone Modeling. One of the major limitations of single-zone modeling is that it does not account for the inherent stratifications that exist within an actual cylinder. Even if the charge can truly be considered homogeneous in composition upon entering the cylinder, the thermal stratifications that develop within the cylinder as heat is transferred to/from the walls, piston, and head will affect how combustion occurs within the cylinder. By the time the piston reaches top dead center (TDC) there will have developed a thermal stratification that is not reflected in a single-zone model. To more accurately model this behavior many researchers have used a multizone modeling approach.[51,53−58]

In the multizone modeling approach, the in-cylinder gases are divided into multiple homogeneous zones (typically 2 to 10 zones), which interact via mass and/or heat transfer. In the present study, a relatively simple approach was taken using the multizone modeling module in CHEMKIN-PRO. The CHEMKIN-PRO multizone approach is based on the work by Aceves et al.[51] but more closely resembles the model by Visakhamoorthy et al.[59] wherein mass and heat is not transferred between zones. Rather, the governing equations are solved for each zone with the stipulation that all zones have the same pressure such that the only communication between zones is that of pressure-work. For the present study, a five-zone approach was used with mass distributed according to Table 6. The mass-distributions for the zones used in this study were determined based on average literature values for multizone models[51,53−59] and distributed across five zones.

Heat transfer to the walls was also included in multizone modeling presented herein. By default, CHEMKIN-PRO has

Table 6. Multi-Zone Model Parameters

zone	core	core	core	boundary layer	boundary layer/crevice
mass[a]	32	24	21	14	9

[a]Percent of total.

only functionality for a Woschni-type heat transfer correlation, but research[50] has shown that other correlations such as those presented by Chang et al.[60] and Hohenberg[61] may be better suited for HCCI operation. Since the model presented by Chang et al. is essentially a modified Woschni correlation, it was possible to use it within the current CHEMKIN-PRO interface. To obtain the proper scaling coefficient for the Chang et al. heat transfer correlation as well as the proper initial temperatures/pressures, the CHEMKIN-PRO model was first matched to a motored-engine pressure curve (Figure 9).

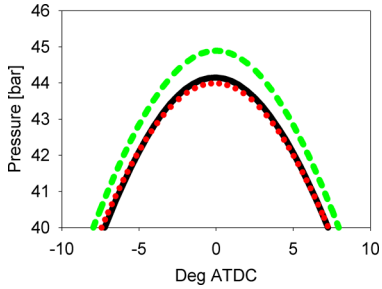

Figure 9. Motored (no fuel) pressure trace with actual data (black solid line), single-zone model without heat transfer (green dashed line), and multizone model with heat transfer (red dotted line).

The heat transfer scaling coefficient from the motored curve was then applied to all of the fuel cases, resulting in good agreement with the experimental data, as shown in Figure 10. In addition to calibrating the heat transfer coefficient to the motored case, the initial in-cylinder temperature and heat transfer area stratification were adjusted proportionally to the zone masses. Specifically, the core zones had the highest temperature and lowest proportional heat transfer area while the boundary layer had the lowest temperature and largest percentage of heat transfer contribution. Overall initial temperature stratification was further adjusted to best fit all of the pressure traces. A zone-average initial in-cylinder temperature at intake valve closure (IVC) of 378 °C was found to give the best agreement for all cases and no zone initial temperature was more than 20 °C from the average value.

Generally the multizone models agree very well with the experimental data, although some small discrepancies are still observed. For the HCCI conditions considered in this study, both the Sarathy* and Mehl et al. mechanisms are reasonably accurate in predicting the location of peak heat release (which corresponds closely to the location of CA50) as well as the point of peak pressure rise for all fuels considered. Alternatively, the Saisirirat et al. mechanism accurately predicts for *n*-heptane, nBuOH40, and nBuOH50 cases but accuracy retards as the fuels become less reactive. The deviations for Saisirirat et al. mechanism for the PRF fuels are likely a result of its *n*-heptane chemistry based on the older Curran et al. mechanism from 2002,[39] while the Mehl et al. mechanism is an updated version with more accurate kinetics. The predicted misfires in the Saisirirat et al. model for nBuOH60 may be due to the lack of validation of the mechanism against engine and ignition studies.

dx.doi.org/10.1021/ef4015982 | *Energy Fuels* 2013, 27, 7778−7789

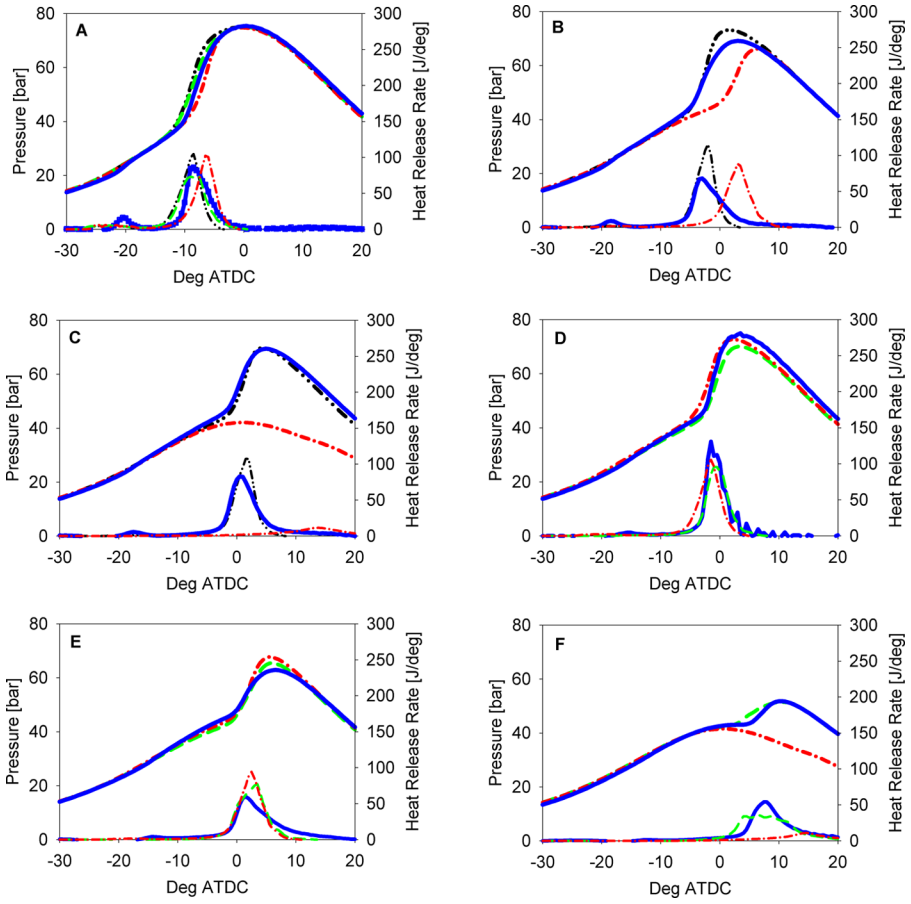

Figure 10. Multizone modeling results: (a) *n*-heptane, (b) PRF40, (c) PRF50, (d) nBuOH40, (e) nBuOH50, (f) nBuOH60. For all figures the solid blue lines are the experimental data, the black dash-dot-dot line is the Mehl et al. model, the red dash-dot line is the Saisirirat et al. model, and the green dashed line is the Sarathy* model.

Additionally, the overall trends observed in the single-zone modeling apply again in the multizone results with the notable exception that the multizone results match the observed pressure rise rate extremely well. In all cases the LTHR data was slightly under predicted with multizone modeling. This mismatch in the ability of multizone modeling is not uncommon[51,62] and is potentially due to the simplified modeling approach taken here where zones do not exchange heat or mass. Incorporating a more physics-based approach is currently a topic of further research.

Lastly, it is important to note that one area this study differs from others is that it was decided to not adjust the model parameters to exactly match the data for each case individually—as is done in many studies. Rather, the goal was to compare the various mechanisms with constant parameters for all cases and to use the overall trends to observe the relationship between low temperature heat release and CA50 timing, which is explored in section 3.4.

3.4. Impact of Low Temperature Heat Release. In a recent study,[10] Rapp and co-workers show that the normalized LTHR release is a good indicator of the compression ratio at which the CA50 point is at 6°ATDC (they showed a linear correlation). In that study, the LHTR was defined as the accumulated heat release occurring at temperatures <1000 K, the high temperature heat release is defined as the heat release that occurs at temperatures >1000 K and the normalized LTHR is defined as the ratio of the LTHR to the HTHR. Though the normalized LTHR of Rapp et al. showed decent correlation to CA50, it was felt that a more appropriate measure would be the fraction of low temperature heat release as a percent of the total heat release. Viewing the LTHR in this manner more fundamentally relates the ignition timing to temperature.

Therefore, in the present work a *fractional* LTHR is defined as the fraction of the total heat release that occurs at "low" temperature (fLTHR). Specifically, we define the fLTHR as the integral of the low temperature heat release spike seen in the net heat release data (as shown more clearly in Figures 7b and 8b) divided by the integral of the entire heat release trace. For all fuels tested, the LTHR was completed by a temperature of 925 K and so this temperature was chosen as the cutoff for the fLTHR integral for all cases. Note that there is some natural uncertainty in calculating a temperature for a given crank angle, which translates into an additional error in calculating the fLTHR. This error is captured by incorporating the measured COV of the engine operating conditions and is included in the error bars for fLTHR shown in all plots below.

In the study by Rapp et al.[10] the normalized LTHR was found to correlate with the compression ratio. In the present work, the measured fLTHR correlates well with the measured CA50 point. This correlation was found in both the HCCI engine test results and numerical modeling results using the Sarathy*/Mehl et al. mechanism (Figure 11). It should also be noted that the Sarathy* model predicts that the relationship between fLTHR and CA50 is not precisely linear. However, the

dx.doi.org/10.1021/ef4015982 | *Energy Fuels* 2013, 27, 7778−7789

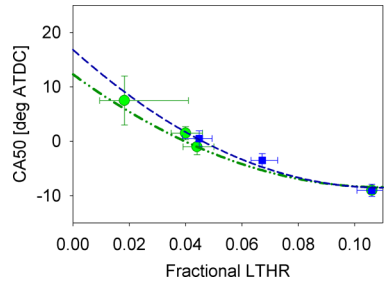

Figure 11. Predicted and measured variation in CA50 as a function of fractional low temperature heat release (fLTHR) for HCCI engine conditions of Table 2. Experimental results are shown for two fuel blends: nBuOH (green circles) and PRF (blue squares). Model results using the Sarathy* and Mehl et al. models are shown for nBuOH (green dashed-dot-dot line) and PRF (blue dashed line).

predicted fLTHR shown spans nBuOH10 to nBuOH60, which represents a wide range of fuel reactivity. Therefore, the correlation between fLTHR and CA50 could potentially be considered linear over a narrower range of fuel reactivity. Lastly, the nBuOH60 did not have a clearly defined LTHR. Indeed, it becomes much more difficult to determine the LTHR for fuels that react in this way although defining a cutoff temperature (such as the 925 K used herein) does give a value for fLTHR. The model predictions for CA50 as a function of fLTHR from the Sarathy*/Mehl et al. mechanism in Figure 11 were shown to vary quadratically with an R^2 value of 0.996. The reasons for this quadratic variation are discussed in the following.

3.5. Relation between fLTHR and CA50. If a relationship exists between fLTHR and CA50, then it might be possible use the fLTHR seen in an FIT (or similar device) to further elucidate the observations seen in HCCI engines. To this end, a first attempt at a phenomenological understanding of the relationship between fLTHR and CA50 is presented in this section. Figure 12a is a plot of temperature history for the

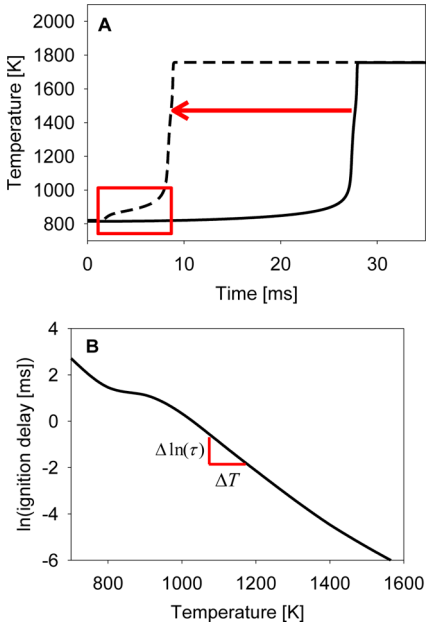

Figure 12. Ignition plots for nBuOH60 showing (a) effect of LTHR on shortening ignition delay for nBuOH60 (dashed line) vs pure nBuOH (solid line), and (b) the Arrhenius-type relation between ln(ignition delay) and temperature for nBuOH60 simulated with Sarathy* at 40 bar and φ = 0.33.

ignition of two fuel blends (nBuOH60 and pure nBuOH) at constant volume for 24 bar initial pressure and 820 K initial temperature (FIT conditions). It is apparent that the nBuOH60 exhibits LTHR, whereas the neat nBuOH exhibits no observable LTHR at these conditions. The net effect of the LTHR for the higher reactivity fuel blend is to raise the temperature of the homogeneous mixture, which results in a reduced ignition delay period before the primary ignition event.

To illustrate how increased fLTHR results in an advance in CA50 in an HCCI engine, one can begin by assuming that the overall ignition delay of a premixed homogeneous fuel/air varies with temperature and pressure according to the Arrhenius form:

$$\tau = AP^{-n}\exp\left(\frac{B}{T}\right) \tag{4}$$

where P is the pressure, T the temperature (which, in an HCCI engine varies with crank angle and therefore time), and A, B, and n are constants. Equation 4 is often presented in the form of an Arrhenius-type plot as shown in Figure 12b for nBuOH60 at 40 bar and ϕ = 0.33. If one assumes that the ignition delay period is only weakly a function of pressure,[63,64] then eq 4 can be simplified as

$$\tau \approx A'\exp\left(\frac{B}{T}\right) \tag{5}$$

In an HCCI engine with ignition behavior that follows eq 4, an Arrhenius plot such as Figure 12b would be valid over some small pressure range such as for several crank angles near top dead center (TDC) in a motored engine cycle. Additionally, Figure 12b is nearly linear for temperatures greater than the negative temperature coefficient (NTC) region, that is, greater than about 900 K for most hydrocarbons. Assuming a linear relation between temperature and ln(ignition delay) allows the derivative

$$\Delta\ln(\tau) = -C * \Delta T \tag{6}$$

where C is a constant equal to the slope of the high temperature section of Figure 12(b). Equation 6 can be rearranged to yield the following relation:

$$\ln(\tau_1) - \ln(\tau_2) = -C(T_1 - T_2)$$

$$\ln\left(\frac{\tau_1}{\tau_2}\right) = C\Delta T_{2-1}$$

$$\tau_1 = \tau_2 \exp(C\Delta T_{2-1}) \tag{7}$$

Equation 7 can be put into the context of an HCCI engine by recognizing that the ignition delays, τ_1 and τ_2 are directly related to crank angles at which the fuel mixture within the cylinder combusts. From Figure 12a, one can see that the time for the mixture to reach full heat release is essentially the same time as for the mixture to reach the 50% heat release, or in other words, the τ can be thought of as the CA50 point for different fuels. The ΔT_{2-1} can be thought of as the fLTHR that shortens the ignition delay relative to the pure component fuel with no LTHR. Furthermore, the fLTHR can be related to the overall heat release via the following:

$$\text{fLTHR} = \frac{\int_{CA_o}^{CA_L} dQ}{\text{Total Heat Release}} = \frac{\int_{T_o}^{T_l} mc_p dT}{\int_{T_o}^{T_f} mc_p dT}$$

$$\approx \frac{T_l - T_o}{(T_f - T_o)} = \frac{\Delta T_{low}}{\Delta T_{total}} \tag{8}$$

dx.doi.org/10.1021/ef4015982 | Energy Fuels 2013, 27, 7778−7789

where CA_L is the crank angle at which low temperature heat release is completed, CA_o is some initial reference crank angle, T_o some initial reference temperature, T_l the temperature at which the fLTHR is completed, and T_f the temperature upon complete heat release and is essentially the maximum temperature seen within the engine. Combining eqs 7 and 8, the final general form relating fLTHR to CA50 is found to be

$$\mathrm{CA50} = \tau_{LR} \exp(C_Q \mathrm{fLTHR}) \tag{9}$$

where τ_{LR} is the CA50 time of the base, low-reactivity, fuel and C_Q is a constant combining the total heat release of the fuel and the slope of the Arrhenius plot. Finally, since fLTHR is a small number, a simplified Taylor series expansion of eq 9 results in the following:

$$\mathrm{CA50} = \tau_{LR}\left(1 + \frac{C_Q \mathrm{fLTHR}}{1!} + \frac{C_Q \mathrm{fLTHR}^2}{2!} + O\left\{\frac{C_Q \mathrm{fLTHR}^3}{3!}\right\}\right) \tag{10}$$

Equation 10 is consistent with the results of Figure 11, which showed that numerical predictions of CA50 varied quadratically with fLTHR.

Since the low temperature heat release occurs at lower pressure it is reasonable to examine the fLTHR as measured at low pressure in the FIT ($\mathrm{fLTHR_{FIT}}$) to see how well it relates to that seen in the engine. To first examine the correlation between the low pressure ignition delay data and the HCCI engine data, the Sarathy* mechanism was again used since model results for FIT and engine conditions can be easily obtained for all fuels. Figure 13 is a plot of the predicted CA50 for HCCI engine model using the Sarathy* mechanism against the fractional low temperature heat release predictions by the same mechanism under FIT conditions ($\mathrm{fLTHR_{24\ bar\text{-}model}}$). A second order polynomial in the form of eq 10 was fit to the data in Figure 13c with an R^2 of 0.99.

In its current configuration, measuring fLTHR directly from the FIT data is difficult because the sample rate at which the pressure data is recorded by the FIT is not sufficient to accurately resolve the LTHR. However, a proxy for this method is proposed. As shown in Figure 5, the FIT-reported ignition delay can be much earlier than the actual ignition delay (as defined by maximum pressure rise rate). As explained above, the FIT measures ignition delay as the time difference between injection and the chamber pressure rising above a set threshold pressure. If one makes the simplifying assumption that the FIT reported ignition delay is proportional to the LTHR then the ratio of the FIT reported ignition delay to the ignition delay found from maximum pressure rise rate ($\mathrm{PRR_{max}}$) of FIT pressure trace should have a linear correlation against the fLTHR. This is indeed the case, as is shown in Figure 13b, which has an R^2 of 0.97. Additionally, the molar blending percentage of low reactivity fuel was found to correlate well with the measured $\mathrm{FIT/PRR_{max}}$ ignition delay ratio (Figure 13a), and so, a linear fit was used to estimate the measured $\mathrm{FIT/PRR_{max}}$ ignition delay for the modeled results in Figure 13b). Molar percentages were thought appropriate since several studies have shown that the reactivity of fuel blends with large quantities of alcohol scaled much more linearly when the mixture was considered on a molar basis,[65,66] as opposed to a volumetric basis.

Using the relationships in Figure 13, an estimated CA50 line can be drawn for the fuels tested based on the measured $\mathrm{FIT/PRR_{max}}$ ignition delays. This relationship shows good agreement with the experimental data as shown in Figure 14.

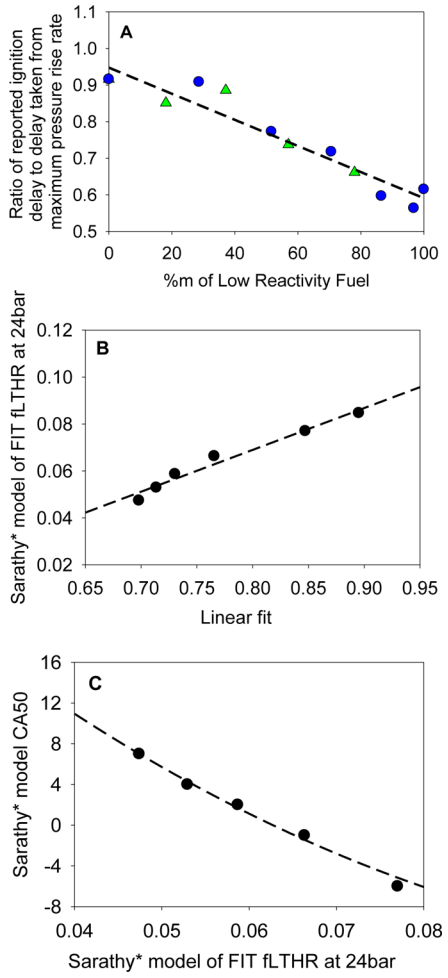

Figure 13. Simple model fits relating FIT to the observed HCCI engine data: (a) molar percent of low reactivity fuel vs measured ratio of FIT-reported to $\mathrm{PRR_{max}}$ ignition delay, R^2 of 0.91 where green triangles are PRF data and blue circles are *n*-butanol/*n*-heptane data, (b) 24 bar FIT model vs $\mathrm{FIT/PRR_{max}}$ ignition delay, R^2 of 0.97, and (c) Sarathy* model CA50 vs 24 bar FIT fLTHR, R^2 of 0.99.

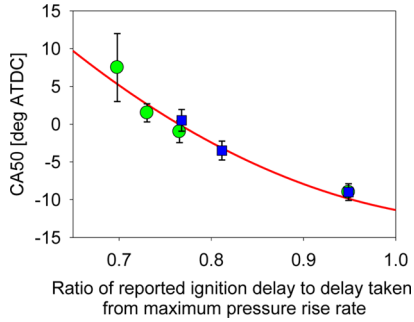

Figure 14. Simple model showing the relation between the ratio of FIT ignition delay to ignition delay found from max PRR curve vs the CA50 found in an HCCI engine: PRF (green circles), *n*BuOH (blue squares), and simplified model (red line).

One caveat to the proposed relationships in Figure 14 is that they are based on the ignition delay data for an *n*-heptane/*n*-butanol blend. A natural outcome of the derivation of eq 10 is that only fuels with similar ignition delay behaviors can be regressed using the same general equations. While there should be a fLTHR-CA50 relationship for every fuel (or fuel blend),

dx.doi.org/10.1021/ef4015982 | Energy Fuels 2013, 27, 7778−7789

the exact equation will depend on the blended fuels such that a given fuel blend may have a different relation; that is, the curves in Figure 11 will shift based on the fuels in the blend. However, it is possible that these relations may be assumed to be rooted in the most and least reactive fuels in the blend. In other words, two different fuel blends may fall on the same blend line if the two fuel blends share the same least and most reactive fuels since these fuels will control the extreme bounds of reactivity.

4. CONCLUSIONS

In this study, two sets of fuel blends were tested in varying amounts of blend ratios in both a FIT and an HCCI engine. Three chemical models were also examined and tested against the experimental data. The Sarathy et al. mechanism, updated to include a current *n*-heptane submechanism by Mehl et al. (dubbed Sarathy*), showed the best ability to model the results obtained from both sets of experiments for both single-zone and multizone models. The FIT accurately reproduced relative fuel ignition rankings, though the magnitude of the differences was greater than that seen in an HCCI engine. However, the FIT experimental data proved quite useful, serving as further support of the accuracy of the examined models at low temperatures. Lastly, the fLTHR showed great promise of being an indicator of CA50 location based on the derivation and data (both experimental and simulation) comparison herein. Investigating the influence of fLTHR and the possibility of obtaining this information from an FIT will be the topic of future research.

AUTHOR INFORMATION

Corresponding Author

*E-mail: Anthony.Marchese@colostate.edu.

Notes

The authors declare no competing financial interest.

ACKNOWLEDGMENTS

This research was funded in part by the National Science Foundation (grant No. 0801707, an NSF IGERT Program in Multidisciplinary Approaches to Sustainable Bioenergy) and the Colorado Center for Biofuels and Biorefining (C2B2). The authors thank Harrison Bucy and Nathan Pekoc for their technical assistance with the FIT as well as Aaron Gaylord, Michael Herder, Scott Salisbury, Ryan Farah, Ryan Peters, and Nathan Zeleski for their assistance in converting the John Deere 4024T engine to operate in HCCI mode. Co-author S.M.S. acknowledges funding from the Clean Combustion Research Center (CCRC) at KAUST and from Saudi Aramco under the FUELCOM research program.

REFERENCES

(1) Dec, J. E. Advanced compression-igniton engines—Understanding the in-cylinder processes. *Proc. Combust. Inst.* **2009**, *32* (2), 2727−2742.

(2) Kokjohn, S. L.; Hanson, R. M.; Splitter, D. A.; Reitz, R. D. Fuel reactivity controlled compression ignition (RCCI): A pathway to controlled high-efficiency clean combustion. *Int. J. Engine Res.* **2010**, *12*, 209−226.

(3) Ciatti, S. The gasoline diesel: Research at a national lab aims to break barriers in fuel economy and emissions performance. *Mechanical Engineering Magazine*; ASME: New York, September 2012.

(4) Lu, X.; Han, D.; Huang, Z. Fuel design and management for the control of advanced compression-ignition combustion modes. *Prog. Energy Combust. Sci.* **2011**, *37* (6), 741−783.

(5) Bessonette, P. W.; Schleyer, C. H.; Duffy, K. P.; Hardy, W. L.; Liechty, M. P. Effects of fuel property changes on heavy-duty HCCI combustion. SAE Technical Paper 2007-01-0191, 2007.

(6) Kaneko, N.; Ando, H.; Ogawa, H.; Miyamoto, N. Expansion of the operating range with in-cylinder water injection in a premixed charge compression ignition engine. SAE Technical Paper 2002-01-1743, 2002.

(7) Koopmans, L.; Stromberg, E.; Dentbratt, I. The influence of PRF and commercial fuels with high octane number on the auto-ignition timing of an engine operated in HCCI combustion mode with negative valve overlap. SAE Technical Paper 2004-01-1967, 2004.

(8) Perez, P. L.; Boehman, A. L. Experimental investigation of the autoignition behavior of surrogate gasoline fuels in a constant-volume combustion bomb apparatus and its relevance to HCCI combustion. *Energy Fuels* **2012**, *26* (10), 6106−6117.

(9) Liu, H.; Yao, M.; Zhang, B.; Zunqing, Z. Influence of fuel and operating conditions on combustion characteristics of a homogeneous charge compression ignition engine. *Energy Fuels* **2009**, *23* (3), 1422−1430.

(10) Rapp, V.; Cannella, W.; Chen, J. Y.; Dibble, R. Predicting fuel performance for future HCCI engines. *Combust. Sci. Technol.* **2013**, *185* (5), 735−748.

(11) Haas, F. M.; Ramcharan, A.; Dryer, F. L. Relative reactivities of the isomeric butanols and ethanol in an ignition quality tester. *Energy Fuels* **2011**, *25* (9), 3909−3919.

(12) Bogin, G. E., Jr.; DeFilippo, A.; Chen, J. Y.; Chin, G.; Luecke, J.; Ratclif, M. A.; Zigler, B. T.; Dean, A. M. Numerical and experimental investigation of *n*-heptane autoignition in the ignition quality tester (IQT). *Energy Fuels* **2011**, *25* (12), 5562−5572.

(13) Bezaire, N.; Wadumesthrige, K.; Ng, K. Y. S.; Salley, S. O. Limitations of the use of cetane index for alternative compression ignition engine fuels. *Fuel* **2010**, *89*, 3807−3813.

(14) Bogin, G. E., Jr.; Osecky, E.; Ratcliff, M. A.; Luecke, J.; He, X.; Zigler, B. T.; Dean, A. M. Ignition quality tester (IQT) investigation of the negative temperature coefficient region of alkane autoignition. *Energy Fuels* **2013**, *27* (3), 1632−1642.

(15) Silke, E. J.; Curran, H. J.; Simmie, J. M. The influence of fuel structure on combustion as demonstrated by the isomers of heptane: A rapid compression machine study. *Proc. Combust. Inst.* **2005**, *30* (2), 2639−2647.

(16) D7170. *Standard Test Method for Determination of Derived Cetane Number (DCN) of Diesel Fuel Oils—Fixed Range Injection Period, Constant Volume Combustion Chamber Method*; ASTM International: West Conshohocken, PA, 2012.

(17) D6890. *Standard Test Method for Determination of Ignition Delay and Derived Cetane Number (DCN) of Diesel Fuel Oils by Combustion in a Constant Volume Chamber*; ASTM International: West Conshohocken, PA, 2012.

(18) Heywood, J. *Internal Combustion Engine Fundamentals*, 1st ed.; McGraw-Hill, Inc.: New York, 1988.

(19) Saxena, S.; Bedoya, I. D. Fundamental phenomena affecting low temperature combustion and HCCI engines, high load limits, and strategies for extending these limits. *Prog. Energy Combust. Sci.* **2013**, *39*, 457−488.

(20) EPA. *EPA Announces E15 Partial Waiver Decision*, EPA-420-F-11-003; U.S. EPA: Washington, DC, 2011.

(21) Dagaut, P.; Sarathy, S. M.; Thomson, M. J. A chemical kinetic study of *n*-butanol oxidation at elevated pressure in a jet stirred reactor. *Proc. Combust. Inst.* **2009**, *32* (1), 229−237.

(22) Dagaut, P.; Togbe, C. Oxidation kinetics of butanol−gasoline surrogate mixtures in a jet-stirred reactor: Experimental and modeling study. *Fuel* **2008**, *87* (15−16), 3313−3321.

(23) Saisirirat, P.; Togbe, C.; Chanchaona, S.; Foucher, F.; Mounaim-Rousselle, C.; Dagaut, P. Auto-ignition and combustion characteristics in HCCI and JSR using 1-butanol/*n*-heptane and ethanol/*n*-heptane blends. *Proc. Combust. Inst.* **2011**, *33* (2), 3007−3014.

(24) Zhang, Y.; Boehman, A. L. Oxidation of 1-butanol and a mixture of *n*-heptane/1-butanol in a motored engine. *Combust. Flame* **2010**, *157* (10), 1816−1824.

(25) Heufer, K. A.; Fernandes, R. X.; Olivier, H.; Beeckmann, J.; Rohl, O.; Peters, N. Shock tube investigations of ignition delays of *n*-butanol at elevated presures between 770 and 1250 K. *Proc. Combust. Inst.* **2011**, *33* (1), 359−366.
(26) Weber, B. W.; Kumar, K.; Zhang, Y.; Sung, C. J. Autoignition of *n*-butanol at elevated pressure and low-to-intermediate temperature. *Combust. Flame* **2011**, *158* (5), 809−819.
(27) Sarathy, S. M.; Vranckx, S.; Yasunaga, K.; Mehl, M.; OBwald, P.; Metcalf, W. K.; Westbrook, C. K.; Pitz, W. J.; Kohse-Hoinghaus, K.; Fernandes, R. X.; Curran, H. J. A comprehensive chemical kinetic combustion model for the four butanol isomers. *Combust. Flame* **2012**, *159* (6), 2028−2055.
(28) Karwat, D. M. A.; Wagnon, S. W.; Wooldridge, M. S.; Westbrook, C. K. On the combustion chemistry of *n*-heptane and *n*-butanol blends. *J. Phys. Chem.* **2012**, *116* (51), 12406−12421.
(29) Zhang, J.; Niu, S.; Zhang, Y.; Tang, C.; Jiang, X.; Hu, E.; Huang, Z. Experimental and modeling study of the auto-igntion of *n*-heptane/*n*-butanol mixtures. *Combust. Flame* **2013**, *160* (1), 31−39.
(30) Zhang, Y.; Boehman, A. L. Impact of biodiesel on NO_x emissions in a common rail direct injection diesel engine. *Energy Fuels* **2007**, *21* (4), 2003−2012.
(31) Lapuerta, M.; Agudelo, J. R.; Prorok, M.; Boehman, A. Bulk modulus of compressibility of diesel/biodiesel/HVO blends. *Energy Fuels* **2012**, *26* (2), 1336−1343.
(32) Varatharajan, K.; Cheralathan, M. Influence of fuel properties and composition on NO_x emissions from biodiesel powered diesel engines: A review. *Renewable Sustainable Energy Rev.* **2012**, *16* (6), 3702−3710.
(33) Pinzi, S.; Rounce, P.; Herreros, J. M.; Tsolakis, A.; Dorado, M. P. The effect of biodiesel fatty acid composition on combustion and diesel engine exhaust emissions. *Fuel* **2013**, *104*, 170−182.
(34) Jin, C.; Yao, M.; Liu, H.; Lee, C. F.; Ji, J. Progress in the production and application of *n*-butanol as a biofuel. *Renewable Sustainable Energy Rev.* **2011**, *15* (8), 4080−4106.
(35) Aleiferis, P. G.; van Romunde, Z. R. An analysis of spray development with iso-octane, *n*-pentane, gasoline, ethanol, and *n*-butanol from a multi-hole injector under hot fuel conditions. *Fuel* **2013**, *105*, 143−168.
(36) *CHEMKIN 10101(×64)*; Reaction Design: San Diego, CA, 2011.
(37) *CHEMKIN-PRO 15101 (×64)*; Reaction Design: San Diego, CA, 2011.
(38) Mehl, M.; Pitz, W. J.; Westbrook, C. K.; Curran, H. J. Kinetic modeling of gasoline surrogate components and mixtures under engine conditions. *Proc. Combust. Inst.* **2011**, *33* (1), 193−200.
(39) Curran, H. J.; Gaffuri, P.; Pitz, W. J.; Westbrook, C. K. A comprehensive modeling study of iso-octane oxidation. *Combust. Flame* **2002**, *129* (3), 253−280.
(40) Dagaut, P.; Togbe, C. Experimental and modeling study of the kinetics of oxidation of ethanol−*n*-heptane mixtures in a jet-stirred reactor. *Fuel* **2010**, *89* (2), 280−286.
(41) Dagaut, P.; Togbe, C. Experimental and modeling study of the kinetics of oxidation of butanol−*n*-heptane mixtures in a jet-stirred reactor. *Energy Fuels* **2009**, *23* (7), 3527−3535.
(42) Liu, W.; Kelley, A. P.; Law, C. K. Non-premixed ignition, laminar flame propagation and mechansim reduction of *n*-butanol, iso-butanol, and methyl butanoate. *Proc. Combust. Inst.* **2011**, *33* (1), 995−1002.
(43) OBwald, P.; Guldenberg, H.; Kohse-Hoinghaus, K.; Yang, B.; Yuan, T.; Qi, F. Combustion of butanol isomers—A detailed molecular beam mass spectrometry investigation of their flame chemistry. *Combust. Flame* **2011**, *158* (1), 2−15.
(44) Hansen, N.; Harper, M. R.; Green, W. H. High-temperature oxidation chemistry of *n*-butanol—Experiments in low-pressure premixed flames and detailed kinetic modeling. *Phys. Chem. Chem. Phys.* **2011**, *13* (45), 20262−20274.
(45) Stranic, I.; Chase, D. P.; Harmon, J. T.; Yang, S.; Davidson, D. F.; Hanson, R. K. Shock tube measurments of ignition delay times for the butanol isomers. *Combust. Flame* **2012**, *159* (2), 516−527.
(46) Ryan, T. Fuel requirements for HCCI engine operation. *Diesel Engine Emissions Reduction (DEER) Conference*, 2002.
(47) Taylor, C. F. *The Internal Combustion Engine in Theory and Practice*, 2nd ed.; MIT Press: Cambridge, MA, 1985; Vol. *1*.
(48) Ferguson, C. R.; Kirkpatrick, A. T. *Internal Combustion Engines*, 2nd ed.; John Wiley & Sons, Inc., 2001.
(49) Torregrosa, A. J.; Olmeda, P. C.; Romero, C. A. Revising engine heat transfer. *Ann. Fac. Eng. Hunedoara* **2008**, *6* (3), 245−265.
(50) Soyhan, H. S.; Yasar, H.; Walmsley, H.; Head, B.; Kalghatgi, G. T.; Sorusbay, C. Evaluation of heat transfer correlations for HCCI engine modelling. *Appl. Therm. Eng.* **2008**, *29* (2−3), 541−549.
(51) Aceves, S. M.; Flowers, D. L.; Westbrook, C. K.; Smith, J. R.; Pitz, W. J. A multi-zone model for prediction of HCCI combustion and emissions. SAE 2000-01-0327, 2000.
(52) *Using Multi-Zone Engine Modeling with Detailed Chemistry for Accurate Ignition and Emissions Predictions in HCCI Engines*, Reaction Design Pro-APP-MZ (v2.0); Reaction Design: San Diego, CA, 2010.
(53) Komninos, N. P.; Hountalas, D. T.; Rakopoulos, C. D. A parametric investigation of hydrogen HCCI combustion using a multi-zone model approach. *Energy Convers. Manage.* **2007**, *48* (11), 2934−2941.
(54) Fiveland, S.; Assanis, D. Development of a two-zone HCCI combustion model accounting for boundary layer effects. SAE Technical Paper 2001-01-1028, 2001.
(55) Easley, W.; Agarwal, A.; Lavoie, G. Modeling of HCCI combustion and emissions using detailed chemistry. SAE Technical Paper 2001-01-1029, 2001.
(56) Noda, T.; Foster, D. A numerical study to control combustion duration of hydrogen-fueled HCCI by using multi-zone chemical kinetic simulation. SAE Technical Paper 2001-01-0250, 2001.
(57) Xu, H.; Liu, M.; Gharahbaghi, S.; Richardson, S.; Wyszynski, M.; Megaritis, T. Modelling of HCCI engines: Comparison of single-zone, mulit-zone, and test data; SAE Technical Paper 2005-01-2123, 2005.
(58) Nobakht, A. Y.; Saray, R. K.; Rahimi, A. A parametric study on natural gas fueled HCCI combustion engine using a multi-zone combustion model. *Fuel* **2011**, *90* (4), 1508−1514.
(59) Visakhamoorthy, S.; Tzanetakis, T.; Haggith, D.; Sobiesiak, A.; Wen, J. Z. Numerical study of a homogeneous charge compression ignition (HCCI) engine fueled with biogas. *Appl. Energy* **2012**, *92*, 437−446.
(60) Chang, J.; Guralp, O.; Filipi, Z.; Assanis, D.; Kuo, T.; Najt, P.; Rask, R. New heat transfer correlation for an HCCI engine derived from measurments of instantaneous surface heat flux. SAE Technical Paper 2004-01-2996, 2004.
(61) Hohenberg, G. F. Advanced approaches for heat transfer calculations; SAE Technical Paper 790825, 1979.
(62) Komninos, N. P. Modeling HCCI combustion: Modification of a multi-zone model and comparison to experimental results at varying boost pressure. *Appl. Energy* **2009**, *86* (10), 2141−2151.
(63) Livengood, J. C.; Wu, P. C. Correlation of autoignition phenomena in internal combustion engines and rapid compression machines. *Fifth Symposium (Int'l) on Combustion*: Reinhold Publishing Corp.: New York, 1955.
(64) Douaud, A. M.; Eyzat, P. Four-octane-number method for predicting the anti-knock behavior of fuels and engines. SAE Technical Paper 780080, 1979.
(65) Foong, T. M.; Morganti, K. J.; Brear, M. J.; da Silva, G.; Yang, Y.; Dryer, F. L. The octane numbers of ethanol blended with gasoline and its surrogates. *Fuel* **2014**, *115*, 727−739.
(66) Anderson, J. E.; Kramer, U.; Mueller, S. A.; Wallington, T. J. Octane numbers of ethanol- and methanol- gasoline blends estimated from molar concentrations. *Energy Fuels* **2010**, *24*, 6576−6585.